Tryptophan−Based Radical in the Catalytic Mechanism of Versatile Peroxidase from Bjerkandera adusta †

ARTICLE *in* BIOCHEMISTRY · APRIL 2005

Impact Factor: 3.02 · DOI: 10.1021/bi047474l · Source: PubMed

10 AUTHORS, INCLUDING:

Rebecca Pogni
Università degli Studi di Siena
103 PUBLICATIONS **1,385** CITATIONS
SEE PROFILE

Brenda Valderrama
Universidad Nacional Autónoma de México
36 PUBLICATIONS **1,213** CITATIONS
SEE PROFILE

Rafael Vazquez-Duhalt
Universidad Nacional Autónoma de México
156 PUBLICATIONS **3,812** CITATIONS
SEE PROFILE

Tryptophan-Based Radical in the Catalytic Mechanism of Versatile Peroxidase from *Bjerkandera adusta*†

Rebecca Pogni,*,‡ M. Camilla Baratto,‡ Stefania Giansanti,‡ Christian Teutloff,§ Jorge Verdin,|| Brenda Valderrama,|| Friedhelm Lendzian,§ Wolfgang Lubitz,⊥ Rafael Vazquez-Duhalt,|| and Riccardo Basosi‡

Department of Chemistry, University of Siena, via Aldo Moro, 53100 Siena, Italy, the Max-Volmer Laboratory for Biophysical Chemistry, Technical University, Berlin, Germany, the Max-Planck-Institute for Bioinorganic Chemistry, Mülheim, Germany, and Instituto de Biotecnologia, UNAM, Apartado Postal 510-3, Cuernavaca, Morelos 62250, Mexico

Received December 2, 2004; Revised Manuscript Received January 18, 2005

ABSTRACT: Versatile peroxidase (VP) from *Bjerkandera adusta* is a structural hybrid between lignin (LiP) and manganese (MnP) peroxidase. This hybrid combines the catalytic properties of the two above peroxidases, being able to oxidize typical LiP and MnP substrates. The catalytic mechanism is that of classical peroxidases, where the substrate oxidation is carried out by a two-electron multistep reaction at the expense of hydrogen peroxide. Elucidation of the structures of intermediates in this process is crucial for understanding the mechanism of substrate oxidation. In this work, the reaction of H_2O_2 with the enzyme in the absence of substrate has been investigated with electron paramagnetic resonance (EPR) spectroscopy. The results reveal an EPR signal with partially resolved hyperfine structure typical of an organic radical. The yield of this radical is ∼30%. Progressive microwave power saturation measurements indicate that the radical is weakly coupled to a paramagnetic metal ion, suggesting an amino acid radical in moderate distance from the ferryl heme. A tryptophan radical was identified as a protein-based radical formed during the catalytic mechanism of VP from *Bjerkandera adusta* through X-band and high-field EPR measurements at 94 GHz, aided by computer simulations for both frequency bands. A close analysis of the theoretical model of the VP from *Bjerkandera* sp. shows the presence of a tryptophan residue near to the heme prosthetic group, which is solvent-exposed as in the case of LiP and other VPs. The catalytic role of this residue in a long-range electron-transfer pathway is discussed.

The extracellular enzymatic system from white rot fungi, which is involved in lignin degradation, consists mainly of oxidative enzymes: laccase, lignin peroxidase (LiP),[1] and manganese peroxidase (MnP) (*1*). However, active lignin-degrading strains of *Pleurotus eryngii* were shown to produce a peroxidase different from *P. chrysosporium* peroxidases, which can both efficiently oxidize Mn^{II} to Mn^{III} and carry out Mn^{II}-independent activity on aromatic substrates (*2*). A related novel manganese−lignin peroxidase hybrid enzyme, called versatile peroxidase (VP), was described for *Bjerkandera* sp. BOS55 and is able to oxidize various phenolic and nonphenolic substrates, such as 2,6-dimethoxyphenol, guaiacol, 2,2′-azinobis-(3-ethylbenzothiazoline-6-sulfonate) (ABTS), and veratryl alcohol (VA), in the absence of Mn^{II} (*3*). Similar VPs have been reported in *Pleurotus eryngii* (*4*−*6*), *Pleurotus pulmonarius* (*7*), *Pleurotus ostreatus* (*8*), as well as in *Bjerkandera adusta* (*3*, *9*−*11*). VPs from *Bjerkandera* and *Pleurotus* species show comparable structural and catalytic parameters, and this allows us to infer the same catalytic intermediates for these enzymes.

VP shows high identity with LiP (58−60%) and MnP (55%) both from *Phanerochaete chrysosporium* (*5*). The heterologous expression of VP in *Aspergillus nidulans* confirmed the ability of this hybrid enzyme to oxidize Mn^{II} and different aromatic compounds in the absence of the mediator (*6*). This enzyme seems to have a long-range electron-transfer pathway similar to those postulated for LiP (*12*, *13*).

Putatively, VP catalyzes the electron transfer from an oxidizable substrate to a hydrogen peroxide molecule following the classic peroxidase mechanism (*14*−*17*). First, in the presence of peroxide, a two-oxidizing equivalent intermediate, compound I, is produced. One-oxidizing equivalent is stored as a ferryl (Fe^{IV}) state with $S = 1$ and the second, as a porphyrin π radical. In some cases, the second oxidizing equivalent is localized on a spatially removed paramagnetic species with $S = {}^1/_2$, namely, a protein-based radical, as the tryptophan radical found in cytochrome *c* peroxidase (*18*). This intermediate is then sequentially reduced back by substrate molecules in a two-step reaction.

† This work was funded by PRIN 2002 (Italy), University of Siena, and CONACYT (Mexico). Financial support by Deutsche Forschungsgemeinschaft DFG (SPP 1051, Le812/3-1 to F.L. and Lu 315/16-2 to W.L.) and German DAAD (VIGONI program, to W.L. and R.B.) is gratefully acknowledged.

* To whom correspondence should be addressed: Telephone: +39-0577-23-4258. Fax: +39-0577-23-4239. E-mail: pogni@unisi.it.

‡ University of Siena.

§ Technical University.

|| UNAM.

⊥ Max-Planck-Institut.

[1] Abbreviations: LiP, lignin peroxidase; MnP, manganese peroxidase; VP, versatile peroxidase; ABTS, 2,2′-azinobis-(3-ethylbenzothiazoline-6-sulfonate); VA, veratryl alcohol; EPR, electron paramagnetic resonance; GPC, gel-permeation chromatography; RNR, ribonuclotide reductase; NBS, *N*-bromosuccinimide.

10.1021/bi047474l CCC: $30.25
Published on Web 02/19/2005

High molecular-weight substrates are unable to directly access the heme edge, and surface residues of the protein may indirectly oxidize them, where the substrate electrons are conducted through an intramolecular pathway to the heme active site. Three different substrate interaction sites and their associated electron-transfer pathways have been proposed for LiP from *P. chrysosporium* (*19*, *20*). However, W171-M172-H176 is the only active electron-transfer pathway experimentally probed (*21*, *22*). Furthermore, in W171 mutants, VA is unable to reduce compounds I and II (*23*−*25*).

The experimental evidence presented in this paper suggests the assignment to a tryptophan residue as the site involved in the long-range electron-transfer pathway. A molecular model based on the sequence of a *Bjerkandera* sp. has been built showing the presence of the Trp170 as the residue that is close to the heme and solvent-exposed.

MATERIALS AND METHODS

Chemicals and Protein Preparation. Potassium hydrogen phthalate, hydrogen peroxide, and succinic acid were purchased from Sigma−Aldrich−Fluka and used without further purification.

VP from *B. adusta* UAMH 8258 was obtained and purified by a method previously described (*10*), in which the modification consisted in an additional chromatographic step on a gel-permeation chromatography (GPC). The partially purified enzyme preparation contained 874 units/mL (105 units/mg protein), measured as manganese peroxidase, and a Reinheitzahl (Rz) value (A_{407}/A_{280}) of 2.3. After the GPC on a sepharose HR-200, the Rz value was incremented to 3.5. LiP activity was estimated by the method of Tien and Kirk (*26*), following the H_2O_2-dependent oxidation of VA to veratrylaldehyde ($\epsilon_{310} = 9300\ M^{-1}\ cm^{-1}$) at 25 °C. Reaction mixtures contained 4 mM VA in 40 mM succinate buffer at pH 3 and were initialized by the addition of H_2O_2 to a final concentration of 0.4 mM. MnP activity was measured by the H_2O_2-dependent formation of a Mn^{III}−malonate complex at 270 nm ($\epsilon = 11\,590\ M^{-1}\ cm^{-1}$). Reactions contained 0.5 mM manganese sulfate in 50 mM malonate buffer (pH 4.5), and the reaction was started by the addition of H_2O_2 to a final concentration of 0.1 mM (*15*). The protein content was determined by the Bio-Rad protein reagent.

Molecular Model. A molecular model for the VP from *Bjerkandera* sp. B33/3 [amino acid sequence deposited in the Swiss Prot. (AA047909.1)] was constructed. The model was obtained by automated homology modeling using LiP (*20*), MnP (*27*), and *Arthromyces ramosus* peroxidase (*28*) as structural templates. After a structural alignment of the target sequence against the templates using Deep View-Swiss PDB viewer version 3.6, the model coordinates were obtained from the Swiss model server (*29*). The model was not refined further.

Electron Paramagnetic Resonance (EPR) Measurements. EPR solutions were prepared with a final concentration of 0.16 mM enzyme and 1.3 mM hydrogen peroxide in 0.1 M phthalate buffer at pH 4.5 (enzyme/hydrogen peroxide molar ratio of 1:8). The reaction was stopped by rapid immersion of the EPR tube in liquid nitrogen after 10 s. CW-X-band (9 GHz) EPR measurements were carried out on a Bruker E500 Elexsys Series using the Bruker ER 4122 SHQE cavity and an Oxford helium continuous flow cryostat (ESR900).

Spin quantification was performed by double integration of the experimental EPR radical signal compared to the iron signal.

High-frequency EPR measurements at 94 GHz were performed in Berlin, Germany, on a Bruker Elexsys 680 spectrometer equipped with a fundamental mode microwave resonator. Spectra were recorded at $T = 40$ K. For determination of precise g-tensor components, the microwave frequency was measured by a frequency counter, which was integrated in the spectrometer. The magnetic field was calibrated with a g standard [Li in LiF, $g = 2.002\,293(2)$ (*30*)] at two different frequencies. All spectra were recorded in the "persistent mode" of the superconducting magnet, using the room-temperature coils for the field sweep to ensure high linearity and stability of the field (maximum sweep width of 80 mT). The modulation amplitude was kept at 0.2 mT to avoid modulation broadening. The design of the 94 GHz EPR microwave resonator ensures high sensitivity and a small active sample dimension (0.7 mm diameter and ∼1.5 mm height) leading to high homogeneity of the magnetic field.

EPR spectra were analyzed using software for simulating and fitting EPR spectra for $S = {}^1/_2$ systems with anisotropic g and hyperfine tensors described in refs *31* and *32*. Thereby, the spectra are simulated by computing the resonant field position correct to the second order at the given microwave frequency, dependent on the orientation of the g and hyperfine tensors with respect to the external magnetic field (*33*, *34*). For the relative orientation of the principal axes of the different tensors, no restriction is applied (*31*).

Microwave Power Saturation Studies. The method of microwave progressive power saturation is commonly used to evaluate electron spin-relaxation times of paramagnetic center in biological systems. Often the aim is to determine the locations of paramagnetic centers in biomolecules by analyzing spin-relaxation enhancements because of long-range spin−spin interaction (*35*). If a protein molecule contains more than one paramagnetic center, magnetic interactions are expected to be dependent on the distance of the centers and on the existence of a special pathway for exchange or superexchange interaction.

The empirical expression used to fit saturation data is

$$S/\sqrt{P} = 1/[1 + (P/P_{1/2})]^{b/2} \qquad (1)$$

where S is the EPR derivative signal amplitude (area) or intensity (height), P is the microwave power, $P_{1/2}$ is the microwave power at half-saturation, and b is the inhomogeneity parameter that varies between 1 (for the inhomogeneous limit) and 3 (for the homogeneous limit). For inhomogeneously broadened lines, the derivative amplitude (S) theoretically increases monotonically to a limiting value with increasing power (P). Homogeneous and inhomogeneous broadening are only the extreme cases encompassing a whole range of intermediate cases (*36*). The inhomogeneous limit ($b = 1$) is the typical case for protein radicals at low temperature. A value of $b < 1$ is diagnostic of a dipolar interaction (*37*).

For the analysis of power saturation data, the log $S/\sqrt{P}$ against log P was plotted. The result is a line parallel to the

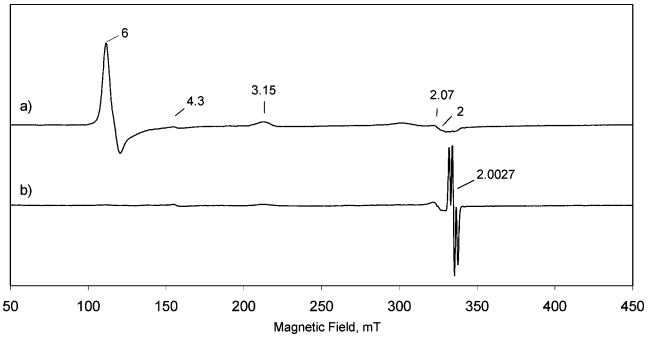

FIGURE 1: Low temperature (20 K) EPR spectra of (a) native VP from *B. adusta* with iron(III) spin states before the addition of H_2O_2 and (b) after the addition of H_2O_2. Both spectra were recorded at ν, 9.390 GHz; modulation amplitude, 1 mT; microwave power, 2 mW; and modulation frequency, 100 kHz.

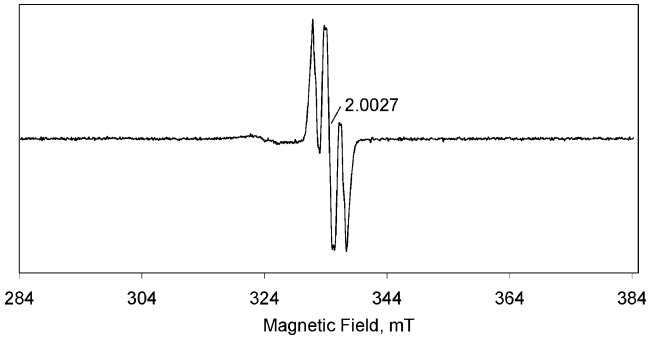

FIGURE 2: Low temperature (20 K) EPR spectrum of the enzyme radical obtained 10 s after the addition of H_2O_2 and rapid freezing in liquid nitrogen. The spectrum was recorded at ν, 9.39 GHz; modulation amplitude, 0.2 mT; microwave power, 2 mW; and modulation frequency, 100 kHz.

abscissa axis, as long as the signal is not saturated, and slopes downward toward the abscissa with increasing saturation. The power for half-saturation is given by the intersection of the extrapolated straight-line portions of the curve (*38*).

RESULTS

Highly pure VP from *B. adusta* was obtained. Protein purity was confirmed by a single electrophoretic band using silver staining and a high Reinheitzahl value (Rz = A_{407}/A_{280}) of 3.5. Spectrophotometric data of the native VP was previously reported and compared with LiP and MnP (*13*).

The X-band EPR spectrum of the resting state of wild-type *Bjerkandera* VP at a temperature of 20 K is shown in Figure 1a. The spectrum is characterized by two distinct signals, indicating the coexistence of a dominant high spin Fe^{III} species ($g_\perp = 6.00$ and $g_\parallel = 2.00$) and some small amount of low spin Fe^{III} species ($g = 3.15$ and 2.07). The third value of the latter species ($g \approx 1.5$) is too weak and broad to be observed. The feature at $g = 4.3$ corresponds to a very small amount of non-heme iron impurity often seen in protein samples (*39*). The Fe^{III} spin states were also confirmed at room temperature by the electronic absorption spectrum (*13*), suggesting no conformational changes after sample freezing. The EPR signal obtained after the addition of an excess of H_2O_2 (1:8 enzyme/H_2O_2 molar ratio) and rapid cooling, is shown in Figure 1b. The ferric high- and low-spin species disappeared almost completely and were replaced by an intense new radical-like signal, centered at $g = 2.0027$. This is similar to other heme proteins for which a mechanism involving compound I was proposed and where also radical signals were observed instead of a porphyrin radical (*40*−*42*). After 10 s from the addition of H_2O_2, the spin quantitation of the narrow radical signal yielded 0.28 spin/heme.

A close-up of the radical signal is shown in Figure 2. The isotropic signal centered at $g = 2.0027$ has two perfect symmetric peaks at low and high field. A careful analysis of the signal shows that the EPR spectrum is dominated by hyperfine interaction.

The data suggest that, using our experimental conditions (1:8 enzyme/H_2O_2), the reaction of H_2O_2 with the heme proceeds probably via intermediate formation of a very short-lived compound I precursor and rapidly to a radical located on an amino acidic residue. The assumed ferryl−porphyrin radical intermediate precursor is not detected with our freezing time (*40*, *41*), while amino acid radicals were found as 8 ms freeze-quenched intermediates in a recent study of the reaction of P450cam with peroxy acids (*42*).

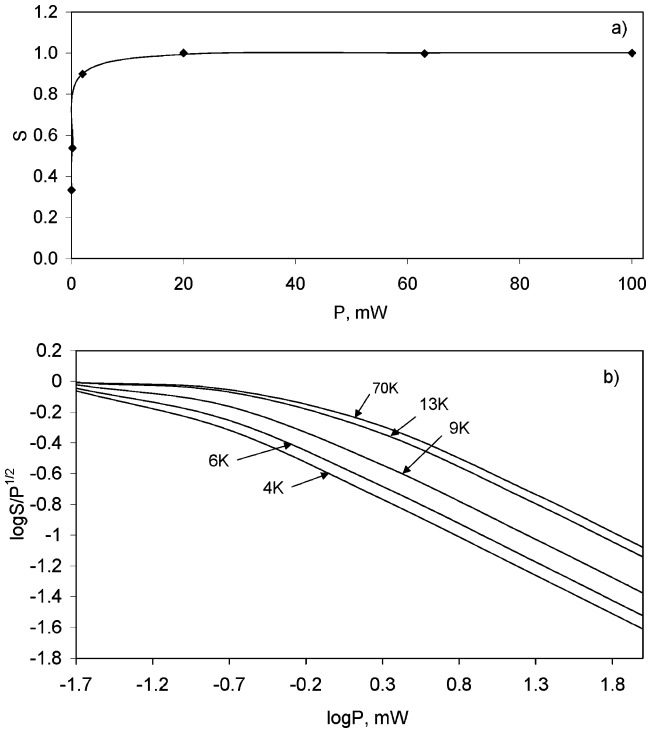

FIGURE 3: (a) Double integration (area, *S*) of the normalized radical signal at $g = 2.0027$ versus microwave power (*P*) (in milliwatts). EPR spectra have been recorded at 70 K; ν, 9.387 GHz; modulation amplitude, 0.2 mT; modulation frequency, 100 kHz; and microwave power values, 0.02, 0.2, 2, 20, 63, and 100 mW. (b) Continuous microwave power saturation curves for the radical signal at $g = 2.0027$ recorded at 4, 6, 9, 13, and 70 K. The log $S/\sqrt{P}$ (where *S* is the area of the normalized derivative signal and *P* is the microwave power) versus log *P* is reported. EPR spectra have been recorded under the same experimental conditions as in a.

Microwave progressive power saturation measurements were carried out on the radical signal. In Figure 3a, the area (*S*) of the normalized radical signal at $g = 2.0027$ versus the microwave power (in milliwatts) at a temperature of 70 K is plotted. The plot is typical for an inhomogeneously broadened line (*43*), because of the presence of two interacting paramagnetic species, a protein radical with $S = {}^1/_2$ and the ferryl (Fe^{IV}-oxo) with a spin state $S = 1$ (44). To analyze the power saturation measurements, a presentation of log

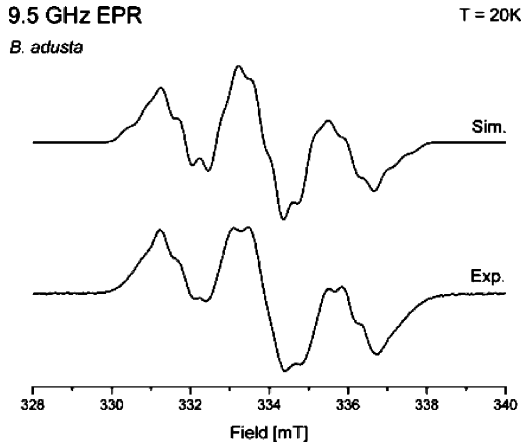

FIGURE 4: Narrow scan of the radical EPR spectrum reported in Figure 2 together with its simulation. Microwave power, 2 mW; modulation amplitude, 0.2 mT; and *T*, 20 K. Parameters are for the simulation and fit, see Table 1.

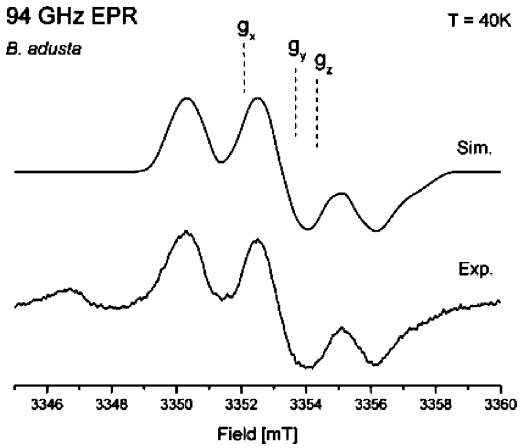

FIGURE 5: EPR spectrum (94 GHz) of the protein radical together with its simulation at $T = 40$ K. Microwave power, 0.25 μW; modulation amplitude, 0.2 mT; and *T*, 40 K. The positions for the three *g*-tensor principal values are shown to indicate the *g* anisotropy in the spectrum. *g*- and hyperfine-tensor components used for the simulation are the same as in Figure 4, see Table 1, except for a somewhat larger intrinsic line width (0.5 mT versus 0.38 mT).

$S/\sqrt{P}$ was plotted against log *P* and the values of $P_{1/2}$ were obtained (Figure 3b). At a temperature of 70 K, the calculated value of *b* (see eq 1) was 0.8. This *b* value is typical for protein radicals at low temperature in the presence of a weak coupling to a paramagnetic ion. The $P_{1/2}$ values obtained from Figure 3b agree well with the value $P_{1/2} = 0.6$ mW at $T =$ 70 K, reported for a tyrosyl radical in P450cam, that is coupled to a ferryl heme iron at about a 7.5 Å distance (*42*). At low temperature, the $P_{1/2}$ values are indicative of a saturated signal even at low microwave power as reported by Khindaria and Aust (*45*). Care was taken to avoid saturation when recording hyperfine-resolved EPR spectra used for spectra simulations, see Figure 4.

In Figure 4, the well-resolved narrow scan EPR radical spectrum together with its simulation is shown. To our knowledge this type of radical has not been reported in the literature for any other peroxidase. It can be clearly seen that the observed EPR signal reveals a partially resolved structure, which is due to nuclear hyperfine interactions. The signal is centered at a *g* value of 2.0027(1), which is a value typical of an organic radical with no spin density on heavier atoms such as oxygen or sulfur. The low experimental g_{iso} value is consistent with the assignment of the signal to an aromatic heterocycle composed of carbon and nitrogen (*46*, *47*). This low g_{iso} value, and the absence of tyrosines [which can have a similar relaxation behavior, when weakly coupled to a ferryl heme iron, and also can show similar X-band EPR spectra as tryptophan radicals (*46*)] in the amino acid sequence of VP (*11*) suggest an assignment of this EPR signal to a tryptophan radical.

Radicals immobilized in proteins can be characterized by their *g*-tensor values that are not affected by different geometries such as, side-chain orientations. In fact, the *g* tensor is a fingerprint for the particular type of radical, which may be used to identify different radicals even in cases where different protein environments induce changes of the hyperfine structure (*46*). Nitrogen-heterocycle radicals, such as the histidine or tryptophan radical, typically show small shifts of their *g*-tensor components $|\Delta g_i| = |g_i - g_e|$ ($i = x, y$, and *z* and free electron value $g_e = 2.002\,319$) of ≤ 0.002 (*40*, *46*, *48*, *49*). Furthermore, for a planar π radical, the shift for the out of plane component, $|\Delta g_z|$, is much smaller than for the in-plane components, $|\Delta g_x|$ and $|\Delta g_y|$ (*49*), because g_z is usually close to the g_e value. Hence, the *g*-tensor principle values provide a molecular fingerprint for the respective type of radical. To determine the small *g*-tensor components of the radical in *B. adusta* more precisely, W-band EPR experiments have been performed.

In Figure 5 the high field W-band EPR spectrum is shown together with its simulation. The obtained *g* values are listed together with the hyperfine-tensor components in Table 1.

A comparison with earlier experimental data on other enzymes shows that the *g*-tensor values of the radical in *B. adusta* are identical within experimental error margins with those from a tryptophan neutral radical observed in mutant Y122F of ribonucleotide reductase (RNR) (refs *31* and *46*, see Table 1). The obtained hyperfine tensor data indicate the presence of two large rather isotropic couplings, typical for β protons of a side chain, two protons with large hyperfine anisotropy, typical for protons attached to an aromatic ring, and a large uniaxial hyperfine coupling from a $S = 1$ ^{14}N nucleus. Again, these values are identical within their experimental error margins with those of the tryptophan radical in refs *31* and *46*. These results strongly suggest an assignment to a tryptophan radical. The weak broad feature on the low-field side of the 94 GHz EPR spectrum might be due to weak coupling to Fe^{IV} ($S = 1$) of the heme, even if this type of feature needs further investigations. It is important to note that both simulations for the X-band and the W-band EPR spectra were done with the same set of *g*- and hyperfine-tensor components. The simulations and fits of the 94 GHz EPR spectrum are more sensitive to the *g*-tensor values, whereas the hyperfine-tensor values of the smaller couplings are obtained from the simulation of the 9.5 GHz EPR spectrum. This multifrequency approach is indispensable for obtaining a unique set of hyperfine- and *g*-tensor values. On the basis of these multifrequency data, we are able to assign the nature of the radical formed during the catalytic mechanism.

DISCUSSION

Recently, EPR signals assigned to uncoupled tryptophan radicals in RNR mutants have been reported (*31*, *46*).

Table 1: Magnetic Parameters for the Tryptophan Radical in the VP from *B. adusta* in Comparison with Tryptophan Radical W111• in RNR of *E. coli*

	B. adusta (this work)			W111• in RNR of *E. coli* (*46*)			spin densities		
tensors	*xx*	*yy*	*zz*	*Xx*	*Yy*	*Zz*	ρ_{exp} (this work)[a]	ρ_{calc} (*31*) neutral[b]	ρ_{calc} (*31*) cation[b]
g[c]	2.0035	2.0025	2.0022	2.0033	2.0024	2.0022	na	na	na
$A_{H\beta1}$[d]	2.15	2.30	2.30	2.70	2.75	2.83	0.52	0.41	0.27
$A_{H\beta2}$[d]	1.75	1.95	1.95	1.38	1.38	1.38	0.52	0.41	0.27
A_{H5}[d,e]	−0.64	≤|0.15|	−0.49	−0.68	≤|0.1|	−0.50	0.17	0.14	0.18
A_{H7}[d,e]	≤|0.15|	−0.62	−0.46	≤|1.0|	−0.61	−0.51	0.16	0.11	0.12
A_N[f]	≤|0.15|	≤|0.15|	1.05	≤|0.15|	≤|0.15|	1.05	0.20	0.23	0.14

[a] π-spin density at the carbon positions C_3, C_5, and C_7, estimated from the experimental hyperfine values, respectively. $H_{\beta1}$ and $H_{\beta2}$ were both used for estimating $\rho(C_3)$, see the text. [b] Theoretical spin densities for carbon positions C_3 (lines $A_{H\beta1}$ and $A_{H\beta2}$), C_5 (A_{H5}), and C_7 (A_{H7}) from earlier DFT calculations (*31*) for the tryptophan neutral radical, deprotonated at N (Chart 1) and for the cation radical, having a proton at N. The experimental values, in particular for C_3 and N, are in favor of a tryptophan neutral radical, see the text. [c] The g values are given with an error of ±0.0001. The g_z axis is expected to be out of the tryptophan plane, according to refs *46* and *50*. The g_x axis is in the tryptophan plane and forms an angle of approximately 20° with the line connecting the center of the C_6-C_7 bond with C_2, see Chart 1 and the text. [d] Hyperfine coupling constants are given in milliteslas, estimated error ±0.1 mT. g and hyperfine-tensor values fit X- and W-band EPR spectra equally well (Figures 4 and 5). Remaining deviations are small and could be a result of weak coupling to the Fe^{IV} ion ($S = 1$ ground state) of the heme. g-tensor and ring proton hyperfine-tensor values (in milliteslas) are similar to those from the tryptophan neutral radical W111• observed previously in RNR (*46*), see columns on the right side. The differences in the hyperfine values of the side-chain protons $H_{\beta1}$ and $H_{\beta2}$ result from different dihedral angles, see the text. [e] Negative sign for ring proton hyperfine values expected from theory in case of positive carbon spin density; for the simulations, the x axes of H_5 and H_7 hyperfine tensors are rotated 30° with respect to the g-tensor x axis, estimated error ±0.05 mT. [f] Axis of $A_{zz}(N)$ is parallel to the g_z axis, as expected for a nitrogen in a planar π system.

Chart 1: Molecular Structure and Numbering Scheme for a Tryptophan Radical[a]

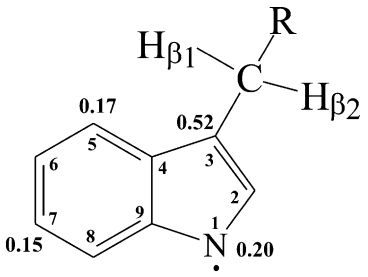

[a] The outer numbers are π-spin densities obtained from the experimental hyperfine values (see the text).

However, in other proteins, electronic coupling of the radical with other paramagnetic centers can obscure the signals (*18*, *48*, *51*−*53*). For the radical in *B. adusta*, the dominant splittings in the spectrum arise from distinct hyperfine couplings of the β-methylene protons β_1 and β_2 at C_β. This carbon atom is attached to position C_3 of the tryptophan ring (see Chart 1). These two protons can be considered as almost magnetically equivalent as seen in Table 1. This is an exception because the hyperfine couplings of these two β protons in other tryptophan radicals, detected so far, generally are different, leading to significantly different EPR spectra (*31*, *46*). This is due to a strong dependence on the orientation of the side chain, measured as dihedral angle θ for each of the β protons according to the Heller−McConnell relation (*46*, *49*)

$$A_{iso}(H_\beta) = \rho^\pi_C (B' + B'' \cos^2 \theta) \qquad (2)$$

where ρ^π_C is the carbon spin density, B' and B'' are empirical constants, and θ is the dihedral angle between the adjacent π-carbon (α-carbon) p_z axis and the projected $C_\beta H_\beta$ bond. The dihedral angles of both β protons of the side chain become equivalent when the first carbon−carbon bond of the side chain lies either exactly in the tryptophan ring plane or perpendicular to it. In the first case, the dihedral angle θ for both β protons becomes ≈30° and $\cos^2 \theta \approx 0.75$, whereas in the latter case, the dihedral angle becomes ≈60° for both β protons and $\cos^2 \theta \approx 0.25$. The large and similar magnitudes for both β-proton hyperfine couplings indicate that the side chain is oriented approximately parallel to the tryptophan plane (see below).

Smaller but still partially resolved hyperfine splittings have been observed in tryptophan radicals in mutants of RNR for the protons at ring positions 5 and 7 (Chart 1) and for the nitrogen (*31*, *46*).

Similar subsplittings are also observed in the X-band EPR spectrum on the three major lines of *B. adusta* in Figure 4. The hyperfine-tensor components obtained from the simulation and fit of the spectra shown in Figure 4 are given in Table 1.

The presence of a tryptophan radical as a catalytically active center in VP from *B. adusta* was already suggested from room-temperature EPR measurements in a previous study (*13*). In this previous work, a chemically modified system using *N*-bromosuccinimide (NBS) was analyzed. The NBS reagent is specific for tryptophan residues, because it oxidizes the indole ring to the corresponding oxindole. In this case, a reduction in the catalytic activity of the enzyme (∼85%) was observed.

Two types of tryptophan radicals can in principle be observed. The cation radical, protonated at the nitrogen position, and the neutral radical, deprotonated at the nitrogen, which is then expected to be hydrogen-bonded in a protic environment. Indeed, both forms of radicals were observed as transient intermediates in photolyase (*54*). The data obtained for the tryptophan radical in *B. adusta* are compared in Table 1 with those obtained earlier for the tryptophan neutral radical W111• in mutant Y122F of RNR of *Escherichia coli* (*31*, *46*). All three g-tensor values as well as the hyperfine-tensor components of the ring protons H_5 and H_7 agree very well for both tryptophan radicals. Because of the different dihedral angles for the side-chain β protons, their hyperfine values are different for both radicals. However, when the hyperfine values for both β protons are known, the spin density at C_3 can be calculated from eq 2. For *B. adusta*, the isotropic part $A_{iso} = (A_{xx} + A_{yy} + A_{zz})/3$ is similar

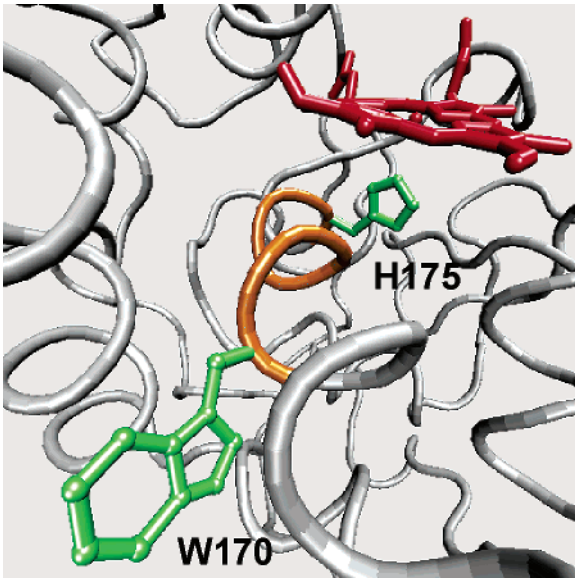

FIGURE 6: Molecular model of the VP from *Bjerkandera* sp. obtained on the structural templates of LiP, MnP, and *A. ramosus* peroxidases [Swiss Prot. (AA047909.1)].

for both β protons, 2.2 mT for $H_{\beta 1}$ and 1.9 mT for $H_{\beta 2}$. Using $B'' = 5.0$ to 5.25 mT (*42*, *55*) and $\theta \approx 30°$ ($\cos^2 \theta \approx 0.75$) from eq 2, a spin density ρ_C^{π} of 0.52−0.54 is estimated for C_3. This agrees well with the value 0.52 given for W111• in ref *46*. Also, the carbon π-spin densities estimated for the ring positons C_5 and C_7 and for the nitrogen agree well with the values reported for the neutral tryprophan radical W111• (see footnote of Table 1). Another orientation where both β-proton hyperfine couplings are equivalent is when the side chain is perpendicular to the molecular plane (see above). In that case, for both β protons, $\theta \approx 60°$ and $\cos^2 \theta \approx 0.25$, which leads to a totally unrealistic spin density of 1.56−1.64 at C_3. We therefore exclude this geometry.

Earlier comparative density functional theory (DFT) calculations for the cation and neutral radical of tryptophan (*31*) showed that the spin densities at C_3 and the nitrogen are significantly different for both radical forms (see right side of Table 1). In particular, the spin density for C_3 based on the clearly resolved large β-proton hyperfine values strongly suggests the neutral form for the tryptophan radical in *B. adusta*.

A catalytically active tryptophan radical has been reported in the literature for several enzymes, e.g., for DNA photolyase, where a coupled tryptophan/flavin radical pair was proposed (*54*, *56*). Interestingly, in photolyase, a chain of successive tryptophan radicals was observed during the electron-transfer reaction. The short-lived intermediate tryptophan radicals inside the protein were reported to be cation radicals, but the longer-lived radical near the surface was a deprotonated tryptophan neutral radical, which is more stable than the cation form (*56*). Similarly, the radical near the surface of VP from *B. adusta* is also a tryptophan neutral radical. However, we want to point out that the catalytically active intermediate radical form in *B. adusta* VP, which reacts with the substrate, could well be the cation radical form, which, in the absence of substrate, is deprotonated to the more stable neutral radical form.

A tryptophan radical center has also been reported for cytochrome *c* peroxidase, where a coupled tryptophan/iron-porphyrin system is observed (*18*), and for ascorbate peroxidase (*57*) and LiP (*21*).

Finally, a molecular model for the VP from *Bjerkandera* sp. B33/3 was constructed. The VP sequence was folded on the structural templates of LiP, MnP, and *A. ramosus* peroxidase. The model shows a solvent-exposed residue, tryptophan (W170). The proposed amino-acid-centered radical is connected to the proximal histidine H175 through a backbone segment (Figure 6), from W170 through L171-L172-A173-S174 to proximal H175. The distance from the α carbon of W170 to the proximal histidine H175 is about 10 Å. The distance from the heme edge to W170 is about 8 Å. The W170 of VP from *Bjerkandera* sp. is analogous to the W171 of LiP from *P. chrysosporium* (*19*, *20*), which is the catalytic residue for the long-range electron-transfer pathway. In addition, residue D181 is placed in the model at 6 Å from the heme propionate and its participation in the long-range electron transfer should not be ruled out.

CONCLUSIONS

In this paper, we focused on the identification and characterization of the radical intermediate formed during the catalytic mechanism of VP from *B. adusta*. Special emphasis is laid on the amino acid residue involved in the catalytic process. On the basis of the EPR results, the observed protein-based radical, was identified as a tryptophan neutral radical. The site is suggested to be W170 in the structural models of VP from *Bjerkandera* sp. B33/3, where this tryptophan residue is both solvent-exposed and placed in proximity (∼10 Å) to the heme.

The presence of this exposed catalytic site in *Bjerkandera* VP accounts for the great capability of this enzyme to degrade bulky and difficult oxidizable substrates also in the absence of a mediator. Substrate oxidation at these sites would depend, mainly, on their redox potential, being an inverse function of the length of the electron-transfer pathway to the heme.

ACKNOWLEDGMENT

The authors are grateful to R. Bittl, Free University, Berlin, Germany, for making available the 94 GHz EPR instrument for this study.

REFERENCES

1. Ten Have, R., and Teunissen, P. J. M. (2001) Oxidative mechanisms involved in lignin degradation by white-rot fungi, *Chem. Rev. 101*, 3397−3413.
2. Martínez, M. J., Ruiz-Dueñas, F. J., Guillén, F., and Martínez, A. T. (1996) Purification and catalytic properties of two manganese peroxidase isoenzymes from *Pleurotus eryngii*, *Eur. J. Biochem. 237*, 424−432.
3. Mester, T., and Field, J. A. (1998) Characterization of a novel manganese peroxidase-lignin peroxidase hybrid isozyme produced by *Bjerkandera* species strain BOS55 in the absence of manganese, *J. Biol. Chem. 273*, 15412−15417.
4. Heinfling, A., Ruiz-Dueñas, F. J., Martínez, M. J., Bergbauer, M., Szewzyk, U., and Martínez, A. T. (1998) A study on reducing substrates of manganese-oxidizing peroxidases from *Pleurotus eryngii* and *Bjerkandera adusta*, *FEBS Lett. 428*, 141−146.
5. Ruiz-Dueñas, F. J., Martínez, M. J., and Martínez, A. T. (1999) Molecular characterization of a novel peroxidase isolated from the ligninolytic fungus *Pleurotus eryngii*, *Mol. Microbiol. 31*, 223−235.
6. Ruiz-Dueñas, F. J., Martínez, M. J., and Martínez, A. T. (1999) Heterologous expression of *Pleurotus eryngii* peroxidase confirms

its ability to oxidize Mn^{2+} and different aromatic substrates, *Appl. Environ. Microbiol. 65*, 4705−4707.
7. Camarero, S., Böckle, B., Martínez, M. J., and Martínez, A. T. (1996) Manganese-mediated lignin degradation by *Pleurotus pulmonarius*, *Appl. Environ. Microbiol. 62*, 1070−1072.
8. Sarkar, S., Martínez, A. T., and Martínez, M. J. (1997) Biochemical and molecular characterization of a manganese peroxidase isoenzyme from *Pleurotus ostreatus*, *Biochim. Biophys. Acta 1339*, 23−30.
9. Heinfling, A., Martínez, M. J., Martínez, A. T., Bergbauer, M., and Szewzyk, U. (1998) Purification and characterization of peroxidases from the dye-decolorizing fungus *Bjerkandera adusta*, *FEMS Microbiol. Lett. 165*, 43−50.
10. Wang, Y., Vazquez-Duhalt, R., and Pickard, M. A. (2001) Effect of growth conditions on the production of manganese peroxidase by three strains of *Bjerkandera adusta*, *Can. J. Microbiol. 47*, 277−282.
11. Wang, Y., Vazquez-Duhalt, R., and Pickard, M. A. (2002) Purification, characterization, and chemical modification of manganese peroxidase from *Bjerkandera adusta* UAMH 8258, *Curr. Microbiol. 45*, 77−87.
12. Camarero, S., Sarkar, S., Ruiz-Dueñas, F. J., Martínez, M. J., and Martínez, A. T. (1999) Description of a versatile peroxidase involved in the natural degradation of lignin that has both manganese peroxidase and lignin peroxidase substrate interaction sites, *J. Biol. Chem. 274*, 10324−10330.
13. Ayala Aceves, M., Baratto, M. C., Basosi, R., Vazquez-Duhalt, R., and Pogni, R. (2001) Spectroscopic characterization of a manganese−lignin peroxidase hybrid isozyme produced by *Bjerkandera adusta* in the absence of manganese: Evidence of a protein centred radical by hydrogen peroxide, *J. Mol. Catal. B: Enzym. 16*, 159−167.
14. Ortiz de Montellano, P. R. (1992) Catalytic sites of hemoprotein peroxidases, *Annu. Rev. Pharmacol. Toxicol.* 32, 89−107.
15. Wariishi, H., Dunford, H. B., MacDonald, I. D., and Gold, M. H. (1989) Manganese peroxidase from the lignin-degrading basidiomycete *Phanerochaete chrysosporium*, *J. Biol. Chem. 264*, 3335−3340.
16. Marquez, L., Wariishi, H., Dunford, H. B., and Gold, M. H. (1988) Spectroscopic and kinetic properties of the oxidized intermediates of lignin peroxidase from *Phanerochaete chrysosporium*, *J. Biol. Chem. 263*, 10549−10552.
17. Valderrama, B., Ayala, M., and Vazquez-Duhalt, R. (2002) Suicide inactivation of peroxidases and the challenge of engineering more robust enzymes, *Chem. Biol. 9*, 555−565.
18. Huyett, J. E., Doan, P. E., Gurbiel, R., Houseman, A. L. P., Sivaraja, M., Goodin, D. B., and Hoffman, B. M. (1995) Compound ES of cytochrome *c* peroxidase contains a trp π-cation radical: Characterization by CW and pulsed Q-band ENDOR spectroscopy, *J. Am. Chem. Soc. 117*, 9033−9041.
19. Schoemaker, H. E., Lundell, T. K., Floris, R., Glumoff, T., Winterhalter, K. H., and Piontek, K. (1994) Do carbohydrates play a role in the lignin peroxidase cycle? Redox catalysis in the endergonic region of the driving force, *Bioorg. Med. Chem. 2*, 509−519.
20. Johjima, T., Itoh, N., Kabuto, M., Tokimura, F., Nakagawa, T., Wariishi, H., and Tanaka, H. (1999) Direct interaction of lignin and lignin peroxidase from *Phanerochaete chrysosporium*, *Proc. Natl. Acad. Sci. U.S.A. 96*, 1989−1994.
21. Choinowski, T., Blodig, W., Winterhalter, K. H., and Piontek, K. (1999) The crystal structure of lignin peroxidase at 1.70 Å resolution reveals a hydroxy group on the C^{β} of tryptophan 171: A novel radical site formed during the redox cycle, *J. Mol. Biol. 286*, 809−827.
22. Blodig, W., Smith, A. T., Doyle, W. A., and Piontek, K. (2001) Crystal structures of pristine and oxidatively processed lignin peroxidase expressed in *Escherichia coli* and the W171F variant that eliminates the redox active tryptophan 171. Implications for the reaction mechanism, *J. Mol. Biol. 305*, 851−861.
23. Blodig, W., Smith, A. T., Winterhalter, K., and Piontek, K. (1999) Evidence from spin-trapping for a transient radical on tryptophan residue 171 of lignin peroxidase, *Arch. Biochem. Biophys. 370*, 86−92.
24. Doyle, W. A., Blodig, W., Veitch, N. C., Piontek, K., and Smith, A. T. (1998) Two substrate interaction sites in lignin peroxidase revealed by site-directed mutagenesis, *Biochemistry 37*, 15097−15105.
25. Timofeevski, S. L., Guojun, N., Scott Reading, N., and Aust, S. D. (2000) Substrate specificity of lignin peroxidase and S168W variant of manganese peroxidase, *Arch. Biochem. Biophys. 373*, 147−153.
26. Tien, M., and Kirk, T. K. (1988) Lignin peroxidase of *Phanerochaete chrysosporium*, *Methods Enzymol. 161*, 238−248.
27. Sundaramoorthy, M., Kishi, K., Gold, M. H., and Poulos, T. L. (1994) The crystal structure of manganese peroxidase from *Phanerochaete chrysosporium* at 2.06 Å resolution, *J. Biol. Chem. 269*, 32759−32767.
28. Kunishima, N., Fukuyama, K., Matsubara, H., Hatanaka, H., Shibano, Y., and Amachi, T. (1994) Crystal structure of the fungal peroxidase from *Arthromyces ramosus* at 1.9 Å resolution, *J. Mol. Biol. 235*, 331−344.
29. Schwede, T., Kopp, J., Guex, N., and Peitsch, M. C. (2003) SWISS-MODEL: An automated protein homology-modeling server, *Nucleic Acids Res. 31*, 3381−3385.
30. Stesmans A., and van Gorp, G. (1989) Novel method for accurate *g* measurements in electron-spin resonance, *Rev. Sci. Instrum. 60*, 2949−2952
31. Lendzian, F., Sahlin, M., MacMillan, F., Bittl, R., Fiege, R., Pötsch, S., Sjöberg, B. M., Gräslund, A., Lubitz, W., and Lassmann, G. (1996) Electronic structure of neutral tryptophan radicals in ribonucleotide reductase studied by EPR and ENDOR spectroscopy, *J. Am. Chem. Soc. 118*, 8111−8120.
32. Schäfer, K. O. (2002) Exchange coupled manganese complexes: Model systems for the active centres in redox proteins investigated with EPR techniques, Ph.D. Thesis, Chemistry Department, Technical University Berlin, Germany.
33. Rieger, P. H. (1982) Least-squares analysis of ESR powder patterns with noncoincident principal axes of the *g* and hyperfine tensors, *J. Magn. Reson. 50*, 485−489.
34. Mombourquette, H. J., and Weil, J. E. (1992) Simulation of magnetic resonance powder spectra, *J. Magn. Reson. 99*, 37−44.
35. Brudvig, G. W. (1995) Electron paramagnetic resonance spectroscopy, *Methods Enzymol. 246*, 536−554.
36. Beinert, H., and Orme-Johnson, W. H. (1967) Electron spin relaxation as a probe for active centers of paramagnetic enzyme species, in *Magnetic Resonance in Biological Systems* (Ehrendberg, A., Malmstrom, B. J., Vanngard, T., Eds.), pp 221−247, Pergamon, Oxford, U.K.
37. Rupp, H., Rao, K. K., Hall, D. O., and Cammack, R. (1978) Electron spin relaxation of iron-sulphur proteins studied by microwave power saturation, *Biochim. Biophys. Acta 537*, 255−260.
38. Galli, C., Innes, J. B., Hirsh, D. J., and Brudvig, G. W. (1996) Effect of dipole−dipole interactions on microwave progressive power saturation of radicals in proteins, *J. Magn. Reson., Ser. B 110*, 284−287.
39. Blumberg, W. E., Peisach, J., Wittenberg, B. A., and Wittenberg, J. B. (1968) The electronic structure of protoheme proteins, *J. Biol. Chem. 243*, 1854−1862.
40. Ivancich, A., Jakopitsch, C., Auer, M., Un, S., and Obinger, C. (2003) Protein-based radicals in the catalase-peroxidase of *Synechocystis* PCC6803: A multifrequency EPR investigation of wild-type and variants on the environment of the heme active site, *J. Am. Chem. Soc. 125*, 14093−14102.
41. Ivancich, A., Mazza, G., and Desbois, A. (2001) Comparative electron paramagnetic resonance study of radical intermediates in turnip peroxidase isozymes, *Biochemistry 40*, 6860−6866.
42. Schünemann, V., Lendzian, F., Jung, C., Contzen, J., Barra, A. L., Sligar, S. G., and Trautwein, A. X. (2004) Tyrosine radical formation in the reaction of wild type and mutant cytochrome P450cam with peroxy acids: A multifrequency EPR study of intermediates on the millisecond time scale, *J. Biol. Chem. 279*, 10919−10930.
43. Weil, J. A., Bolton, J. R., and Wertz, J. E. (1994) Experimental condition, in *Electron Paramagnetic Resonance, Elementary Theory, and Practical Applications*, pp 506−507, Wiley-Interscience, New York.
44. Hoffman, B. M., Roberts, J. E., Hee-Kang, C., and Margoliash, E. (1981) Electron paramagnetic and electron nuclear double resonance of the hydrogen peroxide compound of cytochrome *c* peroxidase, *J. Biol. Chem. 256*, 6556−6564.
45. Khindaria, A., and Aust, S. D. (1996) EPR detection and characterization of lignin peroxidase porphyrin π-cation radical, *Biochemistry 35*, 13107−13111.
46. Bleifuss, G., Kolberg, M., Pötsch, S., Hofbauer, W., Bittl, R., Lubitz, W., Gräslund, A., Lassmann, G., and Lendzian, F. (2001)

Tryptophan and tyrosine radicals in ribonucleutide reductase: A comparative high-field EPR study at 94 GHz, *Biochemistry 40*, 15362−15368.
47. Lassman, G., Eriksson, L. A., Himo, F., Lendzian, F., and Lubitz, W. (1999) Electronic structure of a transient histidine radical in liquid aqueous solution: EPR continuous-flow studies and density functional calculations, *J. Phys. Chem. A 103*, 1283−1290.
48. Miller, J. E., Grădinaru, C., Crane, B. R., Di Bilio, A. J., Wehbi, W. A., Un, S., Winkler, J. R., and Gray, H. B. (2003) Spectroscopy and reactivity of a photogenerated tryptophan radical in a structurally defined protein environment, *J. Am. Chem. Soc. 125*, 14220−14221.
49. McConnell, H. M., and Robertson, R. E. (1957) Spectroscopy splitting factors in aromatic radicals, *J. Phys. Chem. 61*, 1018−1019.
50. Lendzian, F. (2004) Structure and interactions of amino acid radicals in class I ribonucleotide reductase studied by ENDOR and high-field EPR spectroscopy, *Biochim. Biophys. Acta*, in press, published online July 15, 2004.
51. Hori, H., and Yonetani, T. (1985) Powder and single-crystal electron paramagnetic resonance studies of yeast cytochrome *c* peroxidase and its peroxide compound, compound ES*, *J. Biol. Chem. 260*, 349−355.
52. Rigby, S. E. J., Jünemann, S., Rich, P. R., and Heathcote, P. (2000) Reaction of bovine cytochrome *c* oxidase with hydrogen peroxide produces a tryptophan cation radical and a porphyrin cation radical, *Biochemistry 39*, 5921−5928.
53. Sahlin, M., Lassmann, G., Pötsch, S., Slaby, A., Sjöberg, B. M., and Gräslund, A. (1994) Tryptophan radicals formed by iron/oxygen reaction with *Escherichia coli* Ribonucleotide reductase protein M2 mutant Y122F*, *J. Biol. Chem. 269*, 11699−11702.
54. Gindt, Y. M., Vollenbroek, E., Westphal, K., Sackett, H., Sancar, A., and Babcock, G. T. (1999) Origin of the transient electron paramagnetic resonance signals in DNA photolyase, *Biochemistry 38*, 3857−3866.
55. Himo, F., Gräslund, A., and Eriksson, L. A. (1997) Density functional calculations on model tyrosyl radicals, *Biophys. J. 72*, 1556−1567.
56. Aubert, C., Mathis, P., Eker, A. P. M., and Brettel, K. (1999) Intraprotein electron transfer between tyrosine and tryptophan in DNA photolyase from *Anacystis nidulans*, *Proc. Natl. Acad. Sci. U.S.A. 96*, 5423−5427.
57. Hiner, A. N. P., Martínez, J. I., Arnao, M. B., Acosta, M., Turner, D. D., Lloyd-Raven, E., and Rodriguez-Lopez, J. N. (2001) Detection of a tryptophan radical in the reaction of ascorbate peroxidase with hydrogen peroxide, *Eur. J. Biochem. 268*, 3091−3098.

BI047474L